American Mineralogist, Volume 78, pages 1197–1207, 1993

Inferred limitations to the oxidation of Fe in chlorite: A high-temperature single-crystal X-ray study

DANIEL O. NELSON, STEPHEN GUGGENHEIM
Department of Geological Sciences, University of Illinois at Chicago, Chicago, Illinois 60680, U.S.A.

ABSTRACT

The crystal structure of a triclinic ($C\bar{1}$) Mg- and Cr-rich clinochlore-*IIb-4* from the Day Book Body, North Carolina, was determined by refinement of single-crystal X-ray data at 550 °C to $R = 0.083$ and $R_w = 0.084$. Cell parameters were refined at 25, 100, 200, 300, 425, 500, and 550 °C. The crystal was mounted using a new technique that requires no high-temperature cement. Expansion of metric cell dimensions was linear and generally isotropic [mean thermal expansion coefficients (MTEC) of $a = 0.787$, $b = 0.806$, and $c = 0.729 \times 10^{-5}/°$], in contrast to other phyllosilicates, where c expands more than a and b. Comparison with cell parameter data of other Mg- and Fe-rich chlorites shows that expansivity in the [001]* direction may depend on Fe content.

Interlayer separation shows minimal expansion (MTEC = 0.678), indicating that H bonding and electrostatic attractions between the layers are stronger than previously assumed. The M4 site exhibits large expansion (volumetric MTEC > 16) but contains small trivalent cations (Al^{3+}, Cr^{3+}). Because M4 contains trivalent cations, it is the likely site for the oxidation of Fe, but the effect is minimized by site expansion. Ordering trivalent cations into M3 is destabilizing because of M3-M3 and M3-M4 repulsions and other electrostatic repulsions that would lead to the disruption of H bonding, tetrahedral rotation, and lateral expansion of the 2:1 layer. Thus, structure constraints prevent oxidation of Fe from occurring in M3, which has implications in understanding chlorite thermodynamics. Recommendations are made for reporting H positions in phyllosilicates determined with X-ray diffraction.

INTRODUCTION

Because chlorite is an important phase in many different environments, such as greenschist facies and subduction zones, structural and thermodynamic data are important to an understanding of the nature of reactions involving this phase. However, little reliable thermodynamic (Walshe, 1986; Saccocia and Seyfried, 1993) and virtually no structural data are available for chlorite at high temperatures and pressures. These data, however, could involve the development of chlorite as a reliable geothermometer, thereby allowing the assessment of the evolution of geothermal systems and the formation and economic viability of hydrothermal ore deposits (Walshe, 1986). Also, using chlorite to monitor f_{O_2} is a possibility, although recent Mössbauer studies (Dyar et al, 1992; Rancourt, personal communication) have suggested that the oxidation of Fe in chlorite is limited and independent of temperature.

This study characterizes the high-temperature structure of chlorite and provides a crystal chemical model for the structural constraints limiting the oxidation of Fe in chlorite. Although an Fe-poor sample was used, it is structurally analogous to 80% of the commonly occurring chlorites, which includes Fe^{2+}. Furthermore, the presence of Cr^{3+} in this chlorite allows comparison with Fe^{3+}-bearing chlorite. There are no previous high-temperature structure refinements of chlorite and very few (Takeda and Morosin, 1975; Guggenheim et al., 1987) of other hydrous phyllosilicates. This is due primarily to the difficulties of high-temperature single-crystal work, such as dehydroxylation, oxidation, and demanding single-crystal mounting techniques. Because current high-temperature single-crystal mounting techniques are hindered by the problem of cement failure at high temperature, a new technique requiring no cement was developed.

Symmes (1986) studied the effect of increasing temperature on the cell parameters of two chlorite powders to the dehydroxylation temperature of approximately 400–450 °C. He found that the c-axis dimension of the Fe-rich chlorite increased linearly more rapidly than those of the other two axes, but, for the Mg-rich chlorite, the c axis increased linearly at a lesser rate than the lateral axes. The behavior of the Mg-rich sample was considered anomalous because it had not been observed previously. Previous workers (Takeda and Morosin, 1975; Guggenheim et al., 1987) found that the c axis expanded more rapidly than a or b in fluorphlogopite-*1M* and muscovite-$2M_1$, respectively.

0003–004X/93/1112–1197$02.00

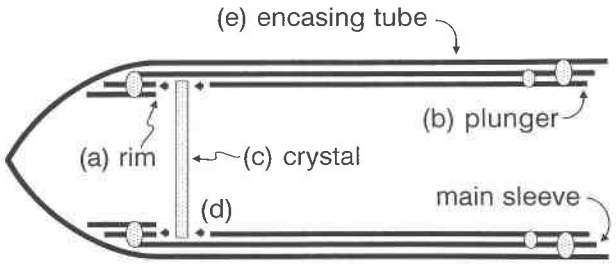

Fig. 1. A schematic longitudinal cross section of the high-temperature crystal mount. The thick solid lines represent nested capillary tubes. The stippled rectangle is the chlorite crystal, with **c*** parallel to the page. The stippled ovals indicate where the quartz-glass tubes have been fused together with an acetylene torch. Although the figure is horizontal, assembly was performed in a vertical orientation. (a) Small cylinders have been fused inside the tip of the main sleeve (0.5 mm in diameter), forming a rim on which the crystal will sit. (b) The plunger is inserted (from the right), leaving space in the tip for manipulation of the crystal. (c) The crystal is inserted through the tip (i.e., from the left, through the hollow center of the small cylinders that form the rim) and teased into position on the rim using a glass fiber. (d) The plunger is pushed into final position (as indicated by the arrows) and fused into place. Thus, the crystal is held in place between the plunger and the rim. (e) The entire assembly is inserted into the encasing tube of 0.7 mm diameter, which is then evacuated and sealed. Sealing is done with an acetylene torch and provides the final weld (at right), which fuses together the three nested tubes.

Experimental

Single-crystal data

A single crystal of chromian clinochlore-*IIb-4* from the Day Book Body, North Carolina, was used for the high-temperature study; see Phillips et al. (1980) for a room-temperature refinement. The sample has a low Fe content, sharp reflections, and minimal streaking of $k \neq 3n$ reflections. The crystal was approximately 0.38 × 0.42 × 0.005 mm in size, with a structural formula of $(Mg_{2.97}Al_{0.03})(Si_{3.02}Al_{0.98})O_{10}(OH)_2 \cdot (Mg_{1.98}Al_{0.69}Cr_{0.23}Fe^{3+}_{0.04}Fe^{2+}_{0.04}Ni_{0.02})(OH)_6$. The absence of $h + k \neq 2n$ reflections in precession photographs confirmed a C-centered unit cell, and space group $C\bar{1}$ was assumed based on the refinement of Phillips et al. (1980).

Mounting technique. The crystal for study was mounted in an evacuated quartz-glass capillary tube, using a technique for platy crystals that does not require high-temperature cement. This eliminates possible crystal movement due to cement failure and diffraction and absorption effects from the cement.

By using melted Crystal Bond glue, silica glass capillary tubes of various diameters were fixed to thin-section slides. A low-speed petrographic saw with a thin diamond blade was used to cut cylinders of varying lengths and diameters with squared-off, butted ends. The Crystal Bond was removed from the resultant silica glass cylinders using acetone. To build the crystal mount (Fig. 1), two of the miniature cylinders were nested, one inside the other, and inserted into the tip of a silica glass capillary tube with an inside diameter of 0.5 mm (the main sleeve). These were fused into place with an acetylene torch. This produces a rim, which acts as a platform, around the inside of the tip of the capillary tube; the plane of the rim or platform is perpendicular to the axis of the encasing capillary tube. Next, a long (2 cm) silica glass cylinder with an outside diameter of 0.5 mm, prepared as described above, was inserted (as a plunger) into the main sleeve from the opposite end. It was positioned approximately 1 mm from the rim, leaving space for manipulation of the crystal. Then, the crystal was loaded into the main sleeve through the hollow center of the small cylinders that form the platform. By leaving an opening at the platform end of the capillary tube, the crystal could be readily teased into position using a glass fiber. The crystal was positioned so that only the corners rested on the platform, much in the same way a playing card can be positioned on top of a glass tumbler with only the corners intersecting the rim. A small dot of the liquid fraction of Zircoa Bond 6 was used to fix the crystal temporarily in position. With the crystal in position, the plunger was pushed fully into the main sleeve. Thus, the crystal is held in place by the corners only, between the opposing rims of the two capillary tubes that constitute the platform and the plunger. Very slight pressure was put on the plunger, and it was then temporarily fixed in place by using a small dot of quick-drying cement at the far end of the encasing tube. The plunger was permanently fused into place using an acetylene torch. The completed assembly was inserted into an encasing tube of 0.7-mm diameter, simultaneously evacuated and heated at 100 °C for 1 h (to remove gases and organics), and then sealed with an acetylene torch. To ensure the integrity of the seal, the evacuated capsule was checked by immersion in liquid. This assembly holds the crystal in the same orientation, as if it were cemented to the tip of a fiber with **c*** parallel to the axis of the fiber. Further data (Guggenheim, unpublished data) show that absorption corrections are improved by fixing the crystal with **c*** perpendicular to the mount axis. This orientation can be achieved by a slight modification of the mount described here.

The portions of the platform and plunger rims that are in physical contact with the crystal constitute 6 and 3% (respectively) of the areas of the two basal cleavage planes assuming complete contact. In fact, because the glass was cut with a saw and is rough, the contact area is smaller. Because there is so little glass in contact with the crystal, it is able to expand as necessary with increasing temperature.

Data measurement. An automated Picker four-circle, single-crystal X-ray diffractometer, with Krisel Control software and equipped with a single-crystal furnace (Brown et al., 1973), was used with graphite monochromatized Mo$K\alpha$ radiation for data measurement. Using least-squares refinement of 160 medium-angle reflections (20 reflections in eight octants), cell parameters were determined at 25, 100, 200, 300, 350, 425, 500, and 550

TABLE 1. Unit-cell parameters to 550 °C

T (°C)	a (Å)	b (Å)	c (Å)	α (°)	β (°)	γ (°)	V (Å^3)
25	5.3219(7)	9.217(2)	14.367(5)	90.23(2)	97.25(2)	89.99(1)	699.1(3)
100	5.3244(5)	9.222(1)	14.372(6)	90.26(2)	97.23(2)	89.98(1)	700.1(3)
200	5.3286(8)	9.228(1)	14.379(8)	90.28(2)	97.22(2)	89.95(1)	701.4(4)
300	5.3322(8)	9.238(2)	14.391(5)	90.23(2)	97.27(2)	90.01(1)	703.2(3)
350	5.3339(9)	9.241(2)	14.395(6)	90.23(2)	97.29(2)	90.01(2)	703.8(4)
425	5.338(1)	9.248(2)	14.403(6)	90.24(3)	97.28(2)	90.04(2)	705.3(4)
500	5.341(1)	9.251(2)	14.411(6)	90.24(3)	97.27(2)	90.02(2)	706.3(4)
550	5.3437(6)	9.256(2)	14.422(7)	90.25(2)	97.28(2)	89.99(2)	707.6(4)

°C (see Table 1). A complete structure refinement was performed at 550 °C, with final unit-cell parameters of a = 5.3437(6), b = 9.256(2), c = 14.422(7) Å, α = 90.25(2)°, β = 97.28(2)°, γ = 89.99(1)°, and V = 707.6(4) Å^3. The furnace was calibrated with the method used by Guggenheim et al. (1987), after the method of Brown et al. (1973), using the melting points of phenoltholein (261 °C), $NaNO_3$ (307 °C), $Ba(NO_3)_2$ (592 °C), and KCl (790 °C). Temperature was controlled and monitored with a Tempstar III temperature controller, with an approximate temperature error of ±3%. Each temperature setting was allowed to equilibrate for 24 h before data measurement was initiated. The intensities of basal spacings, which are very sensitive to interlayer dehydroxylation (Brindley and Ali, 1950), were monitored to ensure that dehydroxylation did not occur.

Four octants of the limiting sphere were sampled in the range h from −7 to 7, k from 0 to 12, and l from −20 to 20, with a scan rate of 1.0°/min, scan window of 2°, and background time of 10 s. The 2θ:θ scan mode was used with three standard reflections monitored every 200 min (approximately every 65 reflections) for electronic stability. Reflections were considered observed if $I > 6\sigma$, where $\sigma(I) = [CT + 0.25(t_c/t_b)^2(B_1 + B_2) + pI)^2]^{1/2}$, and CT is the total integrated count in time t_c, B_1 and B_2 are the background counts in time t_b, and p (the estimate of the standard error) = 0.03. Lorentz-polarization corrections were made, and absorption effects were corrected using a complete ψ scan (0–360° at 10° intervals in ϕ) of the 004 reflection. Of 1954 total reflections measured, 700 reflections with $2\theta > 40°$ and $\chi < 30°$ or $\chi > 150°$ were deleted because of interference by the furnace assembly. The remaining 1254 reflections result in 823 unique nonzero reflections after symmetry averaging. (R_{sym} for the 200 symmetry-redundant reflections was 0.05.) Furthermore, 45 additional reflections were removed according to the equation $\text{abs}(F_o - F_c) > 2[\sigma(F_o - F_c)^2/(M - N)]^{1/2}$, where M = number of reflections and N = number of parameters; thus, 778 unique nonzero intensities were used in the anisotropic refinement. Atomic positions were not changed by removing the 45 reflections, but the standard deviations were much improved. Thus, the resultant displacement factors are considered unreliable. Accordingly, corrections for the effect of displacement factors on calculated bond lengths, such as those suggested by Downs et al. (1992) and Winter et al. (1977), were not made.

Refinement. The room-temperature atomic parameters reported by Phillips et al. (1980) for the Day Book Body chromian clinochlore were used as initial values in the refinement with data from 550 °C. The site occupancies determined by Phillips et al. (1980) were also used, namely, disorder over the tetrahedral sites, ($Mg_{0.99}Al_{0.01}$) in the M1, M2, and M3 sites and Al and remaining Fe ordered in M4. Scattering factor curves were calculated using the method of Sales (1987) and the tables of Cromer and Mann (1968), assuming half-ionization of atoms. The least-squares refinement program SHELXTL PLUS (Siemens, 1990) was used, and reflections were assigned unit weights and a single scale factor. In the initial cycles, the scale factor and atomic positions were varied in space group $C\bar{1}$. Isotropic displacement factors were varied next, followed by anisotropic displacement factors. Site occupancy factors were allowed to vary as a check of scattering factor calculations but were fixed in the final cycles. Final non-H atomic positions were confirmed with a difference-Fourier electron-density (DED) map. Refinement results for the Day Book Body chromian clinochlore structure at 550 °C prior to the determination of H positions are R = 8.5% and R_w = 8.7%, with 130 variable parameters, where $R_w = [\Sigma_w(|F_o| - |F_c|)^2/\Sigma_w|F_c|^2]^{1/2}$.

As the final step in the refinement, a Fourier DED map was used to locate H positions. The standard deviation of the peak, σ, was equal to 0.13 e/Å^3 (by the equation of Ladd and Palmer, 1977, p. 292). Only the ranges of unit-cell space where H atoms should reasonably occur were searched, using resolutions of 0.01, 0.02, and 0.03 Å along the a, b, and c axes, respectively. There were 23 peaks above background (3σ), ranging in height from 0.39 to 0.80 e/Å^3, 12 of which were close to nearby O atoms and could be attributed to poorly described displacement factors of those atoms. Of the remaining 11 peaks, only three resulted in reasonable O-H bond lengths. These represent the H2, H3, and H4 positions, with peak heights 0.47, 0.50, and 0.53 e/Å^3, respectively. In order to obtain a reasonable O-H bond length for the H1 atom, it was necessary to select a peak (0.22 e/Å^3) with a height $<3\sigma$. These four peak heights correspond in position with those reported by Phillips et al. (1980), which were 0.24, 0.41, 0.37, and 0.51 e/Å^3 in height for H1, H2, H3, and H4, respectively. The unrefined coordinates for H are as follows: H1, 0.232, 0.848, 0.142; H2, 0.167, 0.977, 0.360; H3, 0.115, 0.305, 0.367; and H4, 0.616, 0.149, 0.365. Attempts to refine the coordinates were not successful,

TABLE 2. Atomic coordinates and displacement factors at 550 °C

Atom	x	y	z	U_{eq}*	U_{11}**	U_{22}	U_{33}	U_{23}	U_{13}	U_{12}
M1	0.0	0.0	0.0	0.013(2)	0.005(3)	0.006(3)	0.028(3)	−0.001(2)	0.003(2)	0.005(2)
M2	0.0007(6)	0.3337(4)	0.0000(2)	0.012(2)	0.005(2)	0.004(2)	0.029(2)	0.000(1)	0.004(1)	0.004(2)
M3	−0.0008(6)	0.1670(4)	0.5000(3)	0.013(1)	0.005(2)	0.007(2)	0.028(2)	0.000(1)	0.004(1)	0.003(2)
M4	0.0	0.5	0.5	0.036(2)	0.027(3)	0.035(3)	0.047(3)	0.000(2)	0.005(2)	0.002(2)
T1	0.2316(6)	0.1678(3)	0.1914(2)	0.012(1)	0.004(2)	0.007(2)	0.024(2)	−0.001(1)	0.003(1)	0.003(1)
T2	0.7315(6)	0.0011(4)	0.1914(2)	0.014(1)	0.006(2)	0.010(2)	0.028(2)	0.000(1)	0.004(1)	0.006(2)
OH1	0.6915(13)	0.3332(8)	0.0727(5)	0.016(2)	0.004(4)	0.012(5)	0.032(4)	0.000(3)	0.004(3)	0.004(4)
OH2	0.1475(16)	−0.0007(9)	0.4296(6)	0.026(3)	0.024(5)	0.021(5)	0.032(5)	0.000(4)	0.001(4)	−0.001(4)
OH3	0.1405(16)	0.3346(9)	0.4295(5)	0.025(3)	0.030(5)	0.021(5)	0.022(4)	−0.002(3)	0.000(3)	0.002(4)
OH4	0.6403(15)	0.1630(9)	0.4300(6)	0.024(3)	0.019(5)	0.020(5)	0.033(4)	−0.001(4)	0.006(3)	0.010(4)
O1	0.1949(13)	0.1671(8)	0.0772(5)	0.013(2)	0.003(4)	0.009(4)	0.027(4)	0.001(3)	0.002(3)	0.004(3)
O2	0.6938(14)	0.0004(8)	0.0766(5)	0.015(3)	0.006(4)	0.009(4)	0.030(4)	0.001(3)	0.006(3)	0.006(3)
O3	0.2212(16)	0.3325(9)	0.2325(6)	0.029(3)	0.028(6)	0.019(5)	0.041(5)	0.001(4)	0.008(4)	0.002(4)
O4	0.5079(15)	0.0948(10)	0.2323(6)	0.029(3)	0.012(5)	0.032(6)	0.043(5)	0.001(4)	0.005(3)	0.013(4)
O5	0.0102(15)	0.0731(9)	0.2330(6)	0.027(3)	0.023(5)	0.026(6)	0.032(5)	0.000(4)	0.005(3)	−0.006(4)

* $U_{eq} = (1/3) \sum_i \sum_j U_{ij} a_i^* a_j^* \mathbf{a}_i \cdot \mathbf{a}_j$.

** $U_{ij} = \exp\left(-2\pi^2 \sum_i \sum_j U_{ij} a_i^* a_j^* h_i h_j\right)$.

since reasonable bond lengths could not be obtained. Note that the agreement with the coordinates of Phillips et al. (1980) is good. Where these H were included (but not varied) in the structure refinement, the reliability (R) factor decreased from 8.5 to 8.3% (R_w from 8.7 to 8.4%). The exact location of H bonds does not affect the conclusions reached below.

Determining H locations from X-ray data is problematic. Although apparently reasonable in terms of O-H bond length, H positions determined in this manner may not be reliable. A peak height should be $>3\sigma$ above background, yet many studies, including this one, attribute H positions to peak heights $<3\sigma$. Thus, in this study, the H1 peak height is statistically insignificant. Also, the H2, H3, and H4 peak heights are only 0.08–0.14 e/Å^3 above background. Because systematic error results in poorly described displacement factors, it is difficult at this scale to discern DED peaks that have physical meaning from those that are artifacts of systematic error. Accordingly, it is prudent to assume that peaks that occur in possible H positions do not necessarily represent H atoms. Finally, whether accurate or not, H positions added to a refinement reduce the R factor because of the increased number of parameters. Reduction of the R factor in this case does not indicate a more precise structure. Thus, to prevent misleading interpretations of H positions determined using X-ray data, we suggest that the following data should always be reported: (1) the standard deviation (σ) of DED map peak heights, (2) the total number of peaks above background (3σ), and (3) the total number of peaks that, based on bond lengths, represent reasonable H positions. Recognizing that systematic errors are common in absorption corrections for phyllosilicates, the reader can use these parameters to judge whether reported H positions meet the criteria for reliability.

Final atomic and displacement factors are listed in Table 2, and Table 3 compares bond lengths and angles in the structure at 550 °C with those of the room-temperature structure. Structure factor values (F_o and F_c) are listed in Table 4.[1]

Powder data

Symmes (1986) used powder data to study thermal expansion of the unit-cell parameters of a Mg-rich chlorite sample from Quebec and an Fe-rich chlorite sample from Ishpeming, Michigan. To relate data for these chlorite samples to the results of this study, the distributions of elements of high atomic number (in this case, Fe) in the samples used by Symmes were determined. The relative amounts (i.e., degree of asymmetry) of Fe content in the octahedral sheet of the 2:1 layer and interlayer of chlorite can be determined without the necessity of a full structure refinement by comparing the relative intensities of odd-order basal reflections of powders. Bailey (1972) and Brindley and Brown (1984) determined that the method of Petruk (1964) gives the best results, although with an approximate possible error up to 20%. Brindley and Brown (1984) redetermined the curve of Petruk using updated scattering factor and dispersion data.

The samples used by Symmes were powdered and sieved to a particle size <45 μm and mounted (as acetone smears) on zero-background quartz plates. The X-ray data were acquired with a Siemens D5000 automated powder diffractometer in θ:θ configuration, using graphite monochromatized Cu$K\alpha$ radiation and incident- and diffracted-beam slit sizes of 1.0°. Measurements were made from 20 to 40° 2θ, with a 0.02° step and 1.0-s count time. Peak positions and integrated intensities were determined with the Siemens DIFFRAC 5000 Specplot-second-derivative

[1] A copy of Table 4 may be ordered as Document AM-93-542 from the Business Office, Mineralogical Society of America, 1130 Seventeenth Street NW, Suite 330, Washington, DC 20036, U.S.A. Please remit $5.00 in advance for the microfiche.

TABLE 3. Bond lengths and angles at 550 °C and room temperature

Bond lengths (Å)						Bond angles (°)		
	550 °C	25 °C		550 °C	25 °C		550 °C	25 °C
			Tetrahedron T1					
O1	1.634(8)	1.639(4)	O1-O3	2.696(11)	2.716(6)	O1-O3	111.1(4)	110.9(2)
O3	1.637(9)	1.661(4)	O4	2.705(11)	2.713(5)	O4	110.2(4)	110.8(2)
O4	1.664(8)	1.657(4)	O5	2.713(11)	2.712(5)	O5	111.5(4)	110.6(2)
O5	1.648(8)	1.660(4)	O3-O4	2.682(12)	2.684(6)	O3-O4	108.6(4)	108.0(2)
Mean	1.646	1.654	O5	2.654(12)	2.693(6)	O5	107.8(4)	108.4(2)
			O4-O5	2.692(10)	2.686(5)	O4-O5	107.5(4)	108.2(2)
			mean	2.690	2.701	mean	109.4	109.5
			Tetrahedron T2					
O2	1.642(8)	1.641(4)	O2-O3	2.727(11)	2.716(5)	O2-O3	110.6(4)	111.0(2)
O3	1.675(9)	1.655(4)	O4	2.710(11)	2.719(6)	O4	111.1(4)	110.8(2)
O4	1.644(8)	1.663(4)	O5	2.724(11)	2.707(5)	O5	110.6(4)	110.6(2)
O5	1.672(8)	1.652(4)	O3-O4	2.682(12)	2.684(6)	O3-O4	107.8(4)	108.0(2)
Mean	1.658	1.653	O5	2.711(11)	2.678(5)	O5	108.2(4)	108.2(2)
			O4-O5	2.670(10)	2.685(5)	O4-O5	108.5(4)	108.2(2)
			mean	2.704	2.698	mean	109.5	109.5
			Octahedron M1					
O1 × 2	2.100(7)	2.082(4)	O1-O2 × 2	3.083(9)	3.072(5)	O1-O2 × 2	95.2(3)	95.0(1)
O2 × 2	2.088(7)	2.085(4)	OH1 × 2	3.091(10)	3.077(5)	OH1 × 2	95.8(3)	95.9(1)
OH1 × 2	2.067(7)	2.057(4)	O2-OH1 × 2	3.085(9)	3.074(5)	O2-OH1 × 2	95.9(3)	95.9(1)
Mean	2.085	2.075	mean (unshared)	3.086	3.074	mean (unshared)	95.6	95.6
			O1-O2 × 2	2.825(10)	2.814(5)	O1-O2 × 2	84.8(3)	85.0(2)
			OH1 × 2	2.795(10)	2.773(5)	OH1 × 2	84.2(3)	84.1(1)
			O2-OH1 × 2	2.784(10)	2.771(5)	O2-OH1 × 2	84.1(2)	84 1(1)
			mean (shared)	2.801	2.786	mean (shared)	84.4	84.4
			Octahedron M4					
OH2 × 2	2.024(8)	1.961(4)	OH2-OH3 × 2	3.111(11)	2.935(5)	OH2-OH3 × 2	97.4(3)	96.7(2)
OH3 × 2	2.030(8)	1.967(4)	OH4 × 2	3.107(11)	2.934(5)	OH4 × 2	97.6(3)	96.9(2)
OH4 × 2	2.016(8)	1.960(4)	OH3-OH4 × 2	3.040(12)	2.940(6)	OH3-OH4 × 2	97.4(3)	97.0(2)
Mean	2.023	1.963	mean (unshared)	3.086	2.936	mean (unshared)	97.5	96.9
			OH2-OH3 × 2	2.677(12)	2.610(5)	OH2-OH3 × 2	82.6(3)	83.3(2)
			OH4 × 2	2.662(12)	2.601(5)	OH4 × 2	82.4(3)	83.1(2)
			OH3-OH4 × 2	2.671(11)	2.603(5)	OH3-OH4 × 2	82.6(2)	83.0(2)
			mean (shared)	2.670	2.605	mean (shared)	82.5	83.1
			Octahedron M2*					
O1	2.102(8)	2.088(4)	O1-O2	3.085(10)	3.080(5)	O1-O2	94.8(3)	95.2(2)
O2	2.089(8)	2.083(4)	OH1	3.077(9)	3.078(5)	OH1	95.8(3)	95.7(2)
OH1	2.067(7)	2.065(4)	O2-OH1	3.095(9)	3.083(5)	O2-OH1	96.2(3)	96.0(2)
O1′	2.085(7)	2.076(4)	O1′-O2′	3.091(9)	3.075(5)	O1′-O2′	95.1(3)	95.3(2)
O2′	2.094(8)	2.085(4)	OH1′	3.093(9)	3.074(5)	OH1′	95.8(3)	96.1(2)
OH1′	2.063(8)	2.057(4)	O2′-OH1′	3.081(10)	3.071(5)	O2′-OH1′	95.7(3)	95.7(2)
Mean	2.083	2.076	mean (unshared)	3.087	3.077	mean (unshared)	95.6	95.7
			O1-O1′	2.833(10)	2.821(7)	O1-O1′	85.1(3)	85.3(2)
			OH1′	2.795(10)	2.773(5)	OH1′	84.3(3)	84.0(2)
			O2-O1′	2.825(10)	2.814(5)	O2-O1′	85.2(3)	85.2(2)
			O2′	2.831(10)	2.819(7)	O2′	85.2(3)	85.1(2)
			OH1-O2′	2.784(10)	2.771(5)	OH1-O2′	84.0(3)	83.8(2)
			OH1′	2.732(10)	2.724(8)	OH1′	82.8(3)	82.7(2)
			mean (shared)	2.800	2.787	mean (shared)	84.4	84.4
			Octahedron M3*					
OH2	2.057(9)	2.072(4)	OH2-OH3	3.045(11)	3.145(6)	OH2-OH3	98.1(4)	98.8(2)
OH3	2.061(8)	2.069(4)	OH4	3.039(11)	3.150(5)	OH4	98.4(4)	99.2(2)
OH4	2.056(9)	2.064(4)	OH2′-OH3′	3.104(12)	3.152(5)	OH2′-OH3′	97.8(4)	99.1(2)
OH2′	2.064(9)	2.068(4)	OH4′	3.113(12)	3.147(5)	OH4′	98.0(4)	99.2(2)
OH3′	2.054(9)	2.075(4)	OH3-OH4	3.112(11)	3.146(5)	OH3-OH4	98.0(4)	99.2(2)
OH4′	2.052(8)	2.065(4)	OH3′-OH4′	3.108(11)	3.145(5)	OH3′-OH4′	98.5(4)	98.9(2)
Mean	2.057	2.069	mean (unshared)	3.087	3.148	mean (unshared)	98.1	99.1
			OH2-OH2′	2.725(12)	2.771(8)	OH2-OH2′	82.8(4)	84.0(2)
			OH3′	2.677(12)	2.610(5)	OH3′	80.9(3)	78.0(2)
			OH3-OH3′	2.717(11)	2.769(8)	OH3-OH3′	82.6(3)	83.9(2)
			O4′	2.671(11)	2.603(5)	OH4′	81.0(3)	78.1(2)
			OH4-OH2′	2.662(12)	2.763(8)	OH4-OH2′	80.8(3)	84.0(2)
			OH4′	2.724(12)	2.601(5)	OH4′	83.0(3)	78.0(2)
			mean (shared)	2.696	2.686	mean (shared)	81.8	81.0

Note: room-temperature data are from Phillips et al. (1980).
* Primed atoms are related to their counterparts by a center of symmetry.

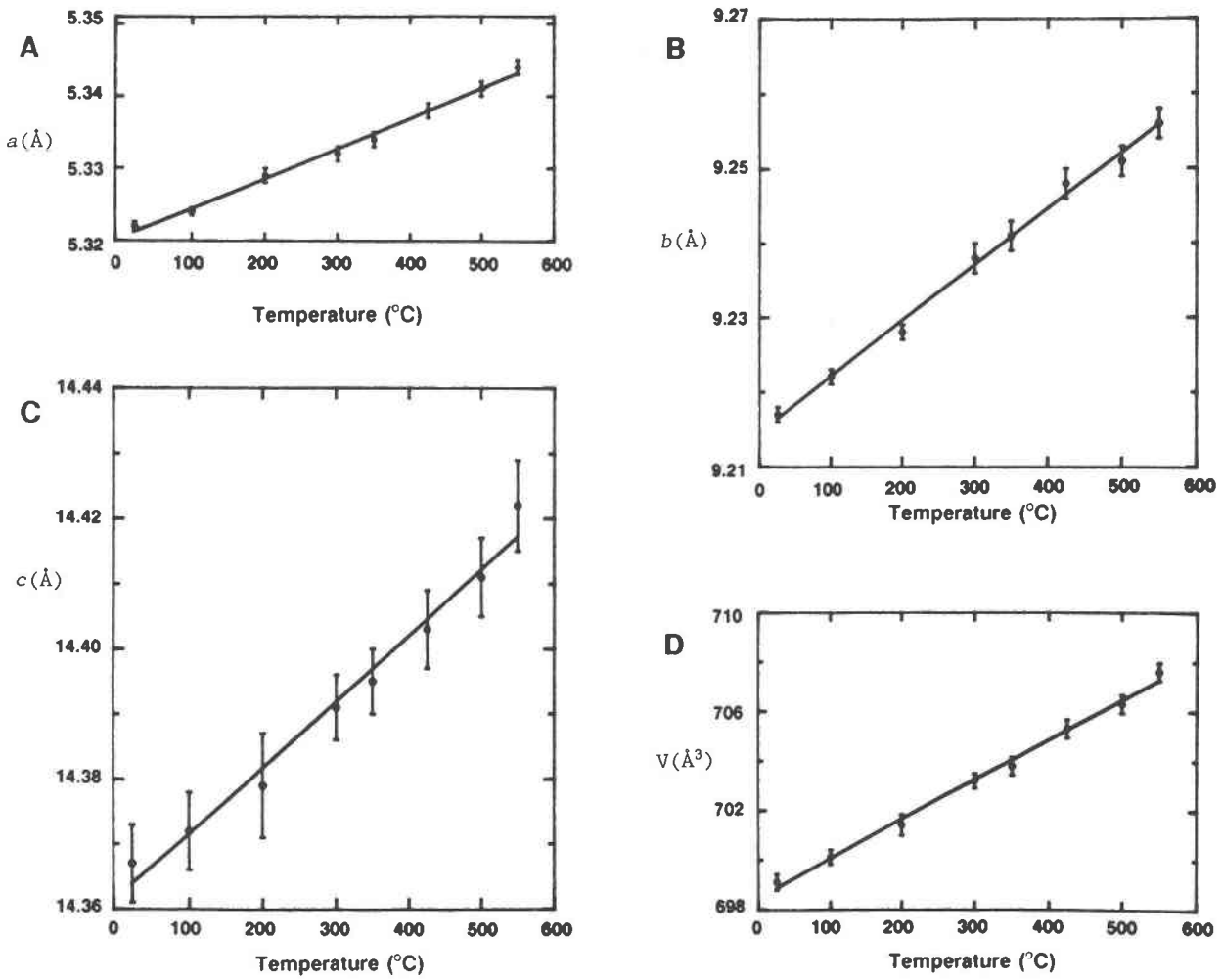

Fig. 2. (A–D) Thermal expansion of unit-cell axes and volume to 550 °C; 1 esd is shown.

search routine, and Fe distributions were calculated by calculating $I(003)/I(005)$ integrated intensity ratios. Structure formulas were derived from the resultant cation distribution based on Brindley and Brown (1984), using the compositions reported for these chlorite samples by Kittrick (1982) and assuming trivalent cations are ordered into M4 and divalent cations into M3 in accord with the results of Phillips et al. (1980). Octahedral vacancies in the Quebec sample were assumed to be equally distributed between the 2:1 layer M1 site and interlayer M4 site. For the Quebec sample, with reported composition of $(Si_{2.99}Al_{1.01})$ $(Al_{1.39}Fe^{3+}_{0.21}Fe^{2+}_{0.57}Mg_{3.52})O_{10}(OH)_8$ and Fe distribution of 0.36 (2:1 layer) and 0.42 (interlayer), $(Mg_{1.73}Al_{0.75}Fe^{2+}_{0.36}\square_{0.16})$ $(Si_{2.99}Al_{1.01})O_{10}(OH)_2 \cdot (Mg_{1.79}Al_{0.64}$-$Fe^{2+}_{0.21}Fe^{3+}_{0.21}\square_{0.15})(OH)_6$is the derived structure formula. For the Michigan sample, with reported composition of $(Si_{2.47}Al_{1.53})(Al_{1.60}Fe^{2+}_{3.29}Mg_{1.05})O_{10}(OH)_8$and Fe distribution of 1.78 (2:1 layer) and 1.51 (interlayer), the derived formula is $(Mg_{0.56}Al_{0.60}Fe^{2+}_{1.78})(Si_{2.47}Al_{1.53})O_{10}(OH)_2 \cdot (Mg_{0.49}$-$Al_{1.00}Fe^{2+}_{1.51})(OH)_6$.

Discussion

Unit-cell parameters

Figure 2 shows the effect of temperature on axial lengths and unit-cell volume. The interaxial angles (Table 1) did not change significantly with temperature, and values are not illustrated, and the d_{001} distance varies with temperature similarly to the c axis, as expected for a nonchanging β angle. There are no significant changes in the slopes of these lines, indicating expansion is constant to 550 °C. These data are in general agreement with those of Symmes (1986).

The relative magnitudes (Table 5) of the mean thermal expansion coefficients (MTEC), however, contrast greatly with those of Symmes (1986). The a, b, and c axial lengths of the Day Book Body clinochlore expand nearly equally, whereas the c axis of the Fe-rich Michigan chlorite expands significantly more than the a and b axes, and the c axis of the Mg-rich Quebec chlorite expands significantly less than the a and b axes. Expansion within the

TABLE 5. Mean thermal expansion coefficients* of compared chlorite samples

Cell parameter	Day Book Body, NC α_{25-550}**	Quebec (21-C)† α_{35-450}**	Ishpeming, MI (21-D)† α_{35-400}**
a	0.787	1.130	0.661
b	0.806	1.018	0.645
c	0.729	0.741	1.385
α	0.042	—	—
β	0.059	0.025	−0.056
γ	0.000	—	—
V	2.316	2.935	2.775
d_{001}	0.722	0.723	1.398

* Values are multiplied by 10^{-5} per degree.

** Values are calculated from $\alpha_{R-T} = (1/X_R)[(X_T - X_R)/(T - R)]$, where X_R and X_T are the values of the parameter at room temperature and higher temperature, respectively.

† Recalculated from Symmes (1986). Values for α and γ were not available, and it is assumed that the unit cell was constrained to be monoclinic.

TABLE 6. Crystal chemical factors vs. c-axis expansion of compared chlorite samples

Parameter	Day Book Body, NC	Quebec (21-C)*	Ishpeming, MI (21-D)*
c-axis MTEC ($\times 10^{-5}$/°)	0.729	0.741	1.385
$^{[6]}Fe^{2+}$, $^{[6]}Fe^{3+}$, $^{[6]}Cr$, $^{[6]}Ni$	0.33	0.78	3.29
$^{[6]}Mg_{tot}$	4.95	3.52	1.05
$^{[6]}Al_{tot}$	0.72	1.39	1.60
2:1 layer $^{[6]}Fe^{2+}$	0.00	0.36	1.78
Interlayer $^{[6]}Fe^{2+}$, $^{[6]}Fe^{3+}$, $^{[6]}Cr$, $^{[6]}Ni$	0.33	0.42	1.51
2:1 layer mean cation charge	2.01	2.14	2.16
2:1 layer mean cation radius (Å)**	0.718	0.682	0.704
M3 mean cation charge	2.04	2.00	2.00
M3 mean cation radius (Å)**	0.718	0.726	0.765
M4 mean cation charge	2.96	3.00	3.00
M4 mean cation radius (Å)**	0.569	0.558	0.535

* MTEC calculated using data from Symmes (1986). Structural formulas were derived from chemical formulas taken from Kittrick (1982).

** Ionic radii were taken from Shannon (1976).

basal plane of the Quebec chlorite is 1.5 times greater than that of the other two samples, although this is probably due to octahedral vacancies in the Quebec sample. An important result is that volumetric expansion in chlorite is variable and not directly related to expansion along the c axis, suggesting that current thermodynamic calculations involving volume changes in chlorite may require adjustment.

In previously studied layer silicates (Guggenheim et al., 1987; Takeda and Morosin, 1975), c-axis thermal expansion is greater than expansion of the lateral dimensions; thus, Symmes suggested that the Mg-rich Quebec chlorite is anomalous. On the contrary, the similarity in c-axis expansivity of the two Mg-rich chlorite samples suggests that the results of Symmes are not anomalous, but rather, thermal expansion is more complex in chlorite than in other phyllosilicates. This is illustrated in Table 6, which compares rates of thermal expansion along the c axis with crystal chemical factors. Although the available data are scant, there are possible correlations. Note that c-axis expansion increases with increasing Fe and Al content, and with decreasing Mg content. Note also that the c axis expands in accordance with $M3$ cation radius, but not with $M4$ or 2:1 layer cation radii. These effects indicate that thermal expansion along **c*** may be directly related to Fe content and is possibly dependent on occupancy of the M3 site.

Structure parameters

Important structure features of both the room-temperature and high-temperature structures are compared in Table 7, and mean thermal expansion coefficients for the various polyhedra and layers are reported in Table 8. Octahedral distortions were calculated using the methods of Dollase (1969) and Robinson et al. (1971).

Tetrahedral rotation, α, which is a measure of the misfit between the tetrahedral and octahedral sheets of the 2:1 layer, decreases from 7.2 to 4.6° (Table 7). Since α does not approach zero, the basal O ring remains ditrigonal at higher temperatures, indicating that tetrahedral rotation is not a limiting factor in lateral expansion to 550 °C. Tetrahedral sites undergo little change, with T2 increasing slightly in size and T1 decreasing slightly. Contraction of tetrahedral sites at higher temperatures is common where corrections for thermal motion are not made (Downs et al., 1992). All other 2:1 layer structure features (Table 6) remain essentially invariant, except for slight increases in the sizes of M1 and M2, implying that thermal expansion in the 2:1 layer is nearly isotropic. The most notable effects of thermal expansion (Tables 7 and 8) are the substantial increase in mean cation-to-anion distances in the interlayer M4 octahedral site (MTEC = 5.887×10^{-5}/°) and the lack of significant increase in interlayer separation (MTEC = 0.678×10^{-5}/°). The 2:1 octahedral sheet thickens only slightly, and the tetrahedral sheet not at all, whereas the interlayer octahedral sheet thickness increases from 1.976 to 2.011 Å (MTEC = 3.374×10^{-5}/°). Only the M4 site, which enlarges at a rate five to six times that of all other sites (Table 8), undergoes significant thermal expansion. Thus, expansion of the structure may be attributed to the interlayer octahedral sheet and specifically to the M4 site. Surprisingly, the interlayer space, which contains the H bonds between the 2:1 and interlayers, does not expand. Previously, c-axis expansion of layer silicates has been generally attributed to weak H (or other) bonds, or fewer numbers of bonds between the layers.

At room-temperature, the M4 octahedron is considerably smaller than the M3 octahedron. This is due to the strong attraction by the trivalent cations in M4 to the OH groups that surround it. Because these OH groups are part of a shared edge between the M4 and M3 octahedra, the result in the M3 octahedron is a shortening of the diagonal (shared) edges and a lengthening of the (unshared) edges that make up the upper and lower basal triads. Therefore, the larger M3 octahedron is severely distorted (Phillips et al., 1980), having $\psi = 61.5°$ and $(\sigma_\theta)^2 = 93.8$ (Table 7), whereas the M4 octahedron is more regular in

TABLE 7. Compared structural features

Parameter		550 °C			Room temperature (Phillips et al., 1980)	
Tetrahedral rotation* $^{[4]}\alpha$ (°)		4.6			7.2	
Tetrahedral angle** $^{[4]}\tau$ (°)	T1:	110.9		T1:	110.7	
	T2:	110.8		T2:	110.8	
Octahedral flattening† $^{[6]}\psi$ (°)	M1:	58.8		M1:	58.8	
	M2:	58.8		M2:	58.8	
	M3:	60.7		M3:	61.5	
	M4:	60.2		M4:	59.8	
Octahedral distortion‡		rms (°)	$(\sigma_\theta)^2$		rms (°)	$(\sigma_\theta)^2$
	M1:	5.0	34.3	M1:	5.0	34.4
	M2:	5.1	34.6	M2:	5.1	35.5
	M3:	7.3	72.8	M3:	8.5	93.8
	M4:	6.6	60.4	M4:	6.1	51.4
Polyhedral site volumes (Å^3)	T1:	2.28		T1:	2.32	
	T2:	2.34		T2:	2.31	
	M1:	11.90		M1:	11.71	
	M2:	11.87		M2:	11.72	
	M3:	11.22		M3:	11.28	
	M4:	10.74		M4:	9.83	
Polyhedral site quadratic elongation§ (λ)	T1:	1.001		T1:	1.000	
	T2:	1.000		T2:	1.000	
	M1:	1.010		M1:	1.010	
	M2:	1.010		M2:	1.010	
	M3:	1.023		M3:	1.029	
	M4:	1.018		M4:	1.015	
Sheet thickness (Å)						
Tetrahedral		2.247			2.247	
2:1 octahedral		2.160			2.147	
Interlayer		2.011			1.976	
Interlayer separation (Å)		2.820			2.810	
Δz_{av}, basal O (Å)		0.009			0.005	
β_{ideal}‖ (°)		97.10			97.11	

Note: all room-temperature values are from Phillips et al. (1980) except octahedral distortions, which were incorrect as reported and have been corrected, and polyhedral site volumes, which were calculated from the data of Phillips et al. (1980).

* The $^{[4]}\alpha = \frac{1}{2}|120° - (\text{mean } O_b\text{-}O_b\text{-}O_b \text{ angle})|$.

** The $^{[4]}\tau = O_a\text{-T-}O_b$ angle. The ideal value is 109.47°.

† The $^{[6]}\psi = \cos^{-1}[\text{oct. thickness}/2(\text{mean M-O,OH angle})]$. The ideal value is 54.73°.

‡ The abbreviation rms $= \left[\sum_{i=1}^{15} (\theta_i - \theta_i)^2\right]^{1/2}$, where θ_i is the observed O-M-O angle and θ_i is the ideal O-M-O angle. This is the rms deviation from ideal values of the 15 octahedral angles, as defined by Dollase (1969). And, $(\sigma_\theta)^2 = \sum_{i=1}^{12} (\theta_i - 90)^2/11$, where θ_i is the observed O-M-O angle, as defined by Robinson et al. (1971).

§ The symbol $\lambda = \sum_{i=1}^{n} [(l/l_o)^2/n]$, where l_o is the M-O or T-O distance of a regular polyhedron of the same volume; l is the M-O or T-O distance, and n is the coordination number, as defined by Robinson et al. (1971). A regular polyhedron has a λ value of 1.0.

‖ The symbol $\beta_{ideal} = 180° - \cos^{-1}(a/3c)$.

shape. However, at high temperature, these OH groups move away from M4, and thus, closer to M3. Both the shared and unshared edges of the M4 octahedron expand, whereas in the M3 octahedron the shared edges expand, but the unshared edges contract slightly. As a result, the M3 octahedron becomes less distorted, although still irregular in shape, and flattened [$(\sigma_\theta)^2 = 72.8$ and $\psi = 60.7°$, respectively], and slightly smaller (volumetric MTEC = -1.018×10^{-5}/°). In the M4 octahedron, flattening and distortion increase slightly [ψ from 59.8 to 60.2° and $(\sigma_\theta)^2$ from 51.4 to 60.4, respectively], and volume expands greatly (MTEC = 16.139×10^{-5}/°). Neither the increased distortion of M4 octahedra nor the decreased size of M3 octahedra are unusual; note (Table 7) that the relative sizes and distortions of M3 and M4 octahedra approach each other. However, the volumetric change in the M4 octahedron is notable. The M4-OH mean bond length (Table 3) changes considerably [from 1.963(4) to 2.023(8) Å], but the M3-OH mean bond length does not [from 2.069(4) to 2.057(9) Å]. The important result of these octahedral adjustments is that the greatly expanding M4 octahedra contain a small (trivalent) cation, implying that there are structural constraints other than cation size that dominate the thermal expansion of the chlorite interlayer.

Structural constraints on octahedral expansion

Two unexpected phenomena occur: the interlayer space does not expand, and the M4 site expands considerably. Guggenheim and Eggleton (1988, p. 685) reviewed the role of H bonds in the misfit and morphology of modulated 1:1 layer silicates and concluded that H bonding and electrostatic attractions are important in layer-to-layer interactions. Furthermore, Bish and Giese (1981) concluded that interlayer bonding energy in chlorite, which

comprises H bond strength and electrostatic attraction due to interlayer charge, is substantially increased by ordering of trivalent cations into M4. The Day Book Body chlorite has trivalent cations ordered into M4, an interlayer charge of +0.95 evu, and a high density of interlayer OH groups. Thus, the lack of expansion in the interlayer space supports the findings of Guggenheim and Eggleton (1988) and Bish and Giese (1981) and suggests that interlayer bonding in chlorite is stronger than previously assumed.

It is useful to consider two aspects of H bonds in chlorite: (1) extensional effects related to expansion along **c***, and (2) torsional effects related to lateral shifts between the 2:1 and interlayers. In the chlorite interlayer space, where there is a high density of H bonds and overall interlayer bonding is strong, extension along **c*** is apparently restricted to approximately 2.8 Å (2.820 Å at 550 °C and 2.810 Å at room temperature). Beyond this limit, decomposition might occur with the loss of H bonding between the layers. Torsional effects, on the other hand, are related to changes in the O-H···O bond angles and OH vectors and allow for in-plane adjustments such as tetrahedral rotation. Torsional adjustments do not necessitate changes in the length of the H bond. For example, Phillips et al. (1980) showed for the room-temperature structure that repulsions between M4 and tetrahedral sites are reduced by slight lateral offsets between the 2:1 and interlayers. Furthermore, Rule and Bailey (1987) concluded that tetrahedral rotation always has the effect of moving acceptor O atoms closer to donor OH groups, shortening H bonds. Thus, while interlayer separation remains static, H bond angles and vectors readjust to maximize structural stability. This effect can be applied to thermal expansion of the M3 and M4 sites in this study.

If OH groups remained closely held to the trivalent cation in M4 upon expansion, M3 would be further distorted and flattened. Because M3 is already severely distorted, further distortion would be energetically unsuitable. Yet, the observed thermal expansion of M4 would also indicate local instability because it leaves a small trivalent cation in a large site. Thus, in an isolated interlayer, there is no apparent crystal chemical rationale that would favor stabilization of one site over the other. However, when the effects of tetrahedral rotation and interlayer H bonding are considered as well, the basis for the observed adjustments becomes clear. At higher temperatures, tetrahedral rotation must decrease to allow for lateral expansion in the 2:1 layer. The basal O atoms of the tetrahedra are linked through H bonds to the upper and lower triads of the interlayer octahedra. Thus, tetrahedral rotation and interlayer octahedral expansion must operate in unison to maintain optimal H bonding between the layers as the lateral dimensions of the structure expand. This is achieved by expansion of M4, which maintains close contact between donor OH groups and acceptor O atoms as tetrahedral rotation decreases at higher temperatures. Conversely, if M3 were to expand, there are adverse consequences. First, OH2 and OH3 would move away from O5 and O3, respectively, and OH4 would move closer to O4. This would lengthen two bonds, OH2-H2···O5 and OH3-H3···O3, and shorten one, OH4-H4···O4, resulting in an overall decrease in stability with regard to optimal bond distances. Second, attraction between donor and acceptor atoms would counteract the direction of tetrahedral rotation. This would cause the observed reduction of tetrahedral rotation (from 7.2 to 4.6°) to be limited, in turn limiting lateral expansion of the 2:1 layer. Thus, M3 expansion results in a less stable structure and hence does not occur. In essence, the effects of tetrahedral rotation, H bonding, and reduced distortion of M3 combine to prop open the M4 site, a circumstance that has important implications for Fe oxidation in chlorite.

TABLE 8. Mean thermal expansion coefficients* for polyhedra and sheet thicknesses

	α_{25-550}**		α_{25-550}**
Tetrahedral sites			
T1-O1	−0.581	T2-O2	0.116
-O3	−2.752	-O3	2.302
-O4	0.805	-O4	−2.176
-O5	−1.377	-O5	2.306
Mean	−0.976	mean	0.637
V	−3.342	*V*	2.442
Octahedral sites			
M1-O1 × 2	1.647	M4-OH2	6.119
-O2 × 2	0.274	-OH3	6.101
-OH1 × 2	0.926	-OH4	5.442
Mean	0.949	mean	5.887
V	3.041	*V*	16.139
M2-O1	1.277	M3-OH2	−1.379
-O2	0.549	-OH3	−0.368
-OH1	0.184	-OH4	−0.736
-O1′	0.826	-OH2′	−1.928
-O2′	0.822	-OH3′	−0.738
-OH1′	0.556	-OH4′	−1.199
Mean	0.702	mean	−1.058
V	2.407	*V*	−1.018
Layer thicknesses			
Tetrahedral	0.000	2:1 octahedral	1.153
Interlayer octahedral	3.374	interlayer separation	0.678

* Values are multiplied by 10^{-5} per degree.

** Values are calculated from $\alpha_{R-T} = (1/X_R)[(X_T - X_R)/(T - R)]$, where X_R and X_T are the values of the parameter at room temperature and higher temperature, respectively. Room-temperature parameters were taken from Phillips et al. (1980).

Oxidation reactions in chlorite

The most important consideration of this study is the application of the results to the common chlorites, 80% of which are of the *IIb* polytype form (Bailey, 1980), with semirandom stacking. Rule and Bailey (1987) and Bish and Giese (1981) used charge-balance arguments and electrostatic calculations (respectively) to conclude that ordering trivalent cations into M4 increases structural stability in chlorite. Bailey (1988) further stated that all trioctahedral chlorites refined up to that time, including the Day Book Body sample, show this ordering to some degree, as well as disorder of Al and Si over the tetrahe-

dral sites. A refinement of an intergrown *IIb-2* and *IIb-4* chlorite (Zheng and Bailey, 1989) demonstrates that this ordering scheme occurs in both of these polytypes and in the random displacements between them. Thus, it follows that the thermal expansion that occurs in the M3 and M4 octahedra of the Day Book Body chlorite also occurs in the common chlorite varieties, including the Fe-rich varieties.

Oxidation in chlorite can be explained by considering the high-temperature structure. Because of the large size of M4 at higher temperatures, a large divalent cation would be more spatially stable in this site. On the basis of this argument, if Fe^{2+} were to occupy M4, it should be resistant to oxidation. On the contrary, M4 is regularly occupied by trivalent cations because (as stated above) this ordering pattern increases the stability of the structure of chlorite. Such ordering (1) minimizes repulsions between M4 and tetrahedral sites and restricts the source of interlayer positive charge to a single site (Rule and Bailey, 1987), and (2) substantially increases interlayer bonding energy (Bish and Giese, 1981). Thus, the M4 site is a likely candidate for oxidation in Fe-rich chlorite. On the other hand, oxidation in M3 at high temperature is highly unlikely, because of charge-balance considerations and crystal-field effects. First, ordering trivalent atoms into M3 to any great extent would counteract the stabilizing effects (see above) of ordering trivalent cations into M4. This would seriously disrupt interlayer H bonding because there would no longer be sufficient numbers of large divalent cations to prop open the interlayer. The M3 and M4 octahedra would contract around their individual trivalent cations, thereby reducing the lateral dimensions of the interlayer and resulting in possible decomposition. Second, destabilizing M3-M3 and M3-M4 repulsions would occur between trivalent cations. Third, Fe^{2+} has an additional crystal-field stabilization energy that Fe^{3+} does not; hence, Fe^{2+} is more stable in M3 than Fe^{3+}. Ultimately, complete interlayer oxidation would require a dioctahedral interlayer, with vacancies in M4 and an *Ia* polytype; essentially, phase transformation to ferric donbassite. Consequently, it is reasonable to conclude that oxidation of Fe^{2+} to Fe^{3+} in the interlayer of chlorite is limited to M4 and cannot proceed significantly in M3.

A limitation on Fe oxidation in chlorite does exist, as indicated by several recent Mössbauer studies (Dyar et al., 1992; Rancourt, personal communication). Although Mössbauer spectroscopy of chlorites remains somewhat unrefined, it is useful in determining Fe^{2+}/Fe^{3+} ratios. Dyar et al. (1992) used Mössbauer data to determine the oxidation state of over 30 chlorite samples from several f_{O_2} regimes. They found that Fe^{3+} content is generally limited to 15% Fe_{tot} and is not dependent on f_{O_2}. Ballet et al. (1985) had similar Fe^{2+}/Fe^{3+} results for four chlorite samples. In contrast, Kodama et al. (1982) and Townsend et al. (1986) studied three chlorite samples that had been altered through chemical oxidation to vermiculite. They found Fe^{3+} contents of 15, 25, and 34% Fe_{tot} prior to alteration and values of 78, 58, 51% (respectively) after alteration. Evidently, the chlorite interlayer will undergo extensive reconfiguration to vermiculite rather than oxidize substantially. Clearly, the controls on chlorite oxidation are crystallographic rather than thermodynamic, and the model described above best accounts for the observed phenomena.

Conclusions

The high-temperature structure of chlorite has fundamental implications for several areas of chlorite thermodynamics. First, careful attention must be given to calculations involving volume changes in chlorite. Unexpectedly, expansion along [001]* may be greatly influenced by strong interlayer H bonding and electrostatic attractions. Unlike in other hydrous phyllosilicates, the *c* axis of Mg-rich chlorites is observed to expand thermally at a lesser rate than *a* and *b*. Thus, chlorites of different chemistries expand at different rates with increasing temperature, and there may be a correlation of expansion along **c*** with increasing Fe content. This information may aid in refining thermodynamic models based on volumetric thermodynamic data, such as the possible role of chlorite in the dehydration of the down-going slab in subduction zones. Second, crystallographic interactions among tetrahedral rotation, H bonding, M3 octahedral distortion, and M4 displacement factors, which combine to stabilize the high-temperature structure, also prevent ordering of trivalent cations into M3. Thus, the relationship of chlorite composition to bulk rock composition is relatively insensitive to f_{O_2}, as suggested by Dyar et al. (1992), because oxidation of Fe^{2+} to Fe^{3+} in the interlayer is largely restricted to the M4 site. These results suggest that a rapid increase in the activity of Fe^{3+} in the system may produce only a small (possibly unmeasurable) change in the Fe^{3+} content of the chlorite phase. Finally, cation ordering and displacement factors in the interlayer of chlorite may be the driving force involved in the formation of solid-state nanoreactions evolving one chlorite layer into a pair of contiguous serpentine layers, as noted, for example, by Baronnet and Onrubia (1988). Further work is needed to determine if this latter suggestion is reasonable.

Acknowledgments

We thank S.W. Bailey of the University of Wisconsin–Madison for the Day Book Body chlorite sample and B.S. Hemingway of the U.S. Geological Survey, Reston, Virginia, for the Quebec and Michigan chlorite samples. We also thank M.F. Brigatti and L. Poppi for reviewing the manuscript. This work was supported in part by NSF grant EAR-90-03688 and by the Petroleum Research Fund, grant ACS-PRF#21974-AC8-C, which is administered by the American Chemical Society.

References cited

Bailey, S.W. (1972) determination of chlorite compositions by X-ray spacings and intensities. Clays and Clay Minerals, 20, 381–388.

——— (1980) Structures of layer silicates. In G.W. Brindley and G. Brown, Eds., Crystal structures of clay minerals and their X-ray identification, p. 1–124. The Mineralogical Society, London.

——— (1988) Chlorites: Structures and crystal chemistry. In Mineralogical Society of America Reviews in Mineralogy, 9, 347–403.

Ballet, O., Coey, J.M.D., and Burke, K.J. (1985) Magnetic properties of sheet silicates: 2:1:1 layer minerals. Physics and Chemistry of Minerals, 12, 370–378.

Baronnet, A., and Onrubia, Y. (1988) Combined powder XRD, HRTEM and AEM studies of mica-chlorite-serpentines-talc mixed-layering and related phase transformation processes. Zeitschrift für Kristallographie, 185, 115.

Bish, D.L., and Giese, R.F., Jr. (1981) Interlayer bonding in II*b* chlorite. American Mineralogist, 66, 1216–1220.

Brindley, G.W., and Ali, S.Z. (1950) Thermal transformations in magnesian chlorites. Acta Crystallographica, 3, 25–30.

Brindley, G.W., and Brown, G. (1984) X-ray diffraction procedures for clay mineral identification. In G.W. Brindley and G. Brown, Eds., Crystal structures of clay minerals and their X-ray identification, p. 305–360. The Mineralogical Society, London.

Brown, G.E., Sueno, S., and Prewitt, C.T. (1973) A new single-crystal heater for the precession camera and four-circle diffractometer. American Mineralogist, 70, 1169–1179.

Cromer, D.T., and Mann, J.B. (1968) X-ray scattering factors computed from numerical Hartree-Fock wave functions. Acta Crystallographica, A24, 321–324.

Dollase, W.A. (1969) Crystal structure and cation ordering of piemontite. American Mineralogist, 54, 710–717.

Downs, R.T., Gibbs, G.V., Bartelmehs, K.L., and Boisen, M.B., Jr. (1992) Variations of bond lengths and volumes of silicate tetrahedra with temperature. American Mineralogist, 77, 751–757.

Dyar, M.D., Guidotti, C.V., Harper, G.D., McKibben, M.A., and Saccocia, P.J. (1992) Controls on ferric iron in chlorite. Geological Society of America Abstracts with Programs, 1992 Annual Meeting, 338 p.

Guggenheim, S., and Eggleton, R.A. (1988) Crystal chemistry, classification, and identification of modulated layer silicates. In Mineralogical Society of America Reviews in Mineralogy, 19, 675–725.

Guggenheim, S., Chang, Y., and Koster van Groos, A.F. (1987) Muscovite dehydroxylation: High-temperature studies. American Mineralogist, 72, 537–550.

Kittrick, J.A. (1982) Solubility of two high-Mg and two high-Fe chlorites using multiple equilibria. Clays and Clay Minerals, 30, 167–179.

Kodama, H., Longworth, G., and Townsend, M.G. (1982) A Mössbauer investigation of some chlorites and their oxidation products. Canadian Mineralogist, 20, 585–592.

Ladd, M.F.C., and Palmer, R.A. (1977) Structure determination by X-ray crystallography, 393 p. Plenum, New York.

Petruk, W. (1964) Determination of the heavy atom content in chlorite by means of the X-ray diffractometer. American Mineralogist, 49, 61–71.

Phillips, T.L., Loveless, J.K., and Bailey, S.W. (1980) Cr^{3+} coordination in chlorites: A structural study of ten chromian chlorites. American Mineralogist, 65, 112–122.

Robinson, K., Gibbs, G.V., and Ribbe, P.H. (1971) Quadratic elongation: A quantitative measure of distortion in coordination polyhedra. Science, 172, 567–570.

Rule, A.C., and Bailey, S.W. (1987) Refinement of the crystal structure of a monoclinic ferroan clinochlore. Clays and Clay Minerals, 35, 129–138.

Saccocia, P.J., and Seyfried, W.E. (1993) The solubility of chlorite solid solutions in 3.2 wt.% NaCl fluids from 300–400 °C, 500 bars. Geochimica et Cosmochimica Acta, in press.

Sales, K.D. (1987) Atomic scattering factors for mixed atom sites. Acta Crystallographica, A43, 42–44.

Shannon, R.D. (1976) Revised effective ionic radii and systematic studies of interatomic distances in halides and chalcogenides. Acta Crystallographica, A32, 751–760.

Siemens (1990) SHELXTL PLUS 4.0. Siemens Analytical X-Ray Instruments, Inc., Madison, Wisconsin.

Symmes, G.H. (1986) The thermal expansion of natural muscovite, paragonite, margarite, pyrophyllite, phlogopite, and two chlorites: The significance of high *T*/*P* volume studies on calculated phase equilibria. B.A. thesis, Amherst College, Amherst, Massachusetts.

Takeda, H., and Morosin, B. (1975) Comparison of observed and predicted structural parameters of mica at high temperature. Acta Crystallographica, B31, 2444–2452.

Townsend, M.G., Longworth, G., and Kodama, H. (1986) Magnetic interaction at low temperature in chlorite and its products of oxidation: A Mössbauer investigation. Canadian Mineralogist, 24, 105–115.

Walshe, J.L. (1986) A six-component chlorite solid solution model and the conditions of chlorite formation in hydrothermal and geothermal systems. Economic Geology, 81, 681–703.

Winter, J.K., Ghose, S., and Okamura, F.P. (1977) A high-temperature study of the thermal expansion and the anisotropy of the sodium atom in low albite. American Mineralogist, 62, 921–931.

Zheng, H., and Bailey, S.W. (1989) The structures of intergrown triclinic and monoclinic *IIb* chlorites from Kenya. Clays and Clay Minerals, 37, 308–316.

Manuscript received February 24, 1993
Manuscript accepted July 27, 1993